



Combining mercury intrusion porosimetry and fractal theory to determine the porous characteristics of wood

Jingyao Zhao¹ · Lin Yang² · Yingchun Cai¹

Received: 18 June 2020 / Accepted: 30 October 2020 / Published online: 16 November 2020
© Springer-Verlag GmbH Germany, part of Springer Nature 2020

Abstract

The understanding of pore characteristics is the basis for studying the macroscopic physical properties of wood. Herein, mercury intrusion porosimetry (MIP) was analyzed in detail as a function of pressure to analyze wood samples. Additionally, fractal analysis was performed from the MIP derived data to establish the relationship between the fractal dimension and the structural parameters. The results demonstrate that in spite of the large variability of the MIP data from different wood species, the overall trend can be approximated. The aperture size ranged from 2.0 nm to 350 μm with a corresponding porosity ranging from 44.26 to 73.18%. The threshold pressure, average pore radius and pore-to-throat ratio extracted from the MIP data can be used as a valid parameter to evaluate the structural characteristics. The fractal dimension values in the corresponding macropore, mesopore and micropore aperture range intervals are 2.978, 2.827 and 2.438, respectively, which indicate a higher degree of pore complexity for larger pores. Negative correlations are observed between the fractal dimension and porosity with R^2 values of 0.85, and in addition, positive correlations are observed between the fractal dimension and the average pore radius and pore-to-throat ratio with corresponding R^2 values of 0.66 and 0.52, respectively.

Introduction

There is a rapidly growing interest in the analysis of pore structure of wood. Numerical modeling of macroscopic physical properties such as permeability, diffusivity, conductivity and electrical resistivity, needs these structural data as

✉ Yingchun Cai
caiyingchunnefu@163.com

¹ Key Laboratory of Bio-Based Material Science and Technology (Ministry of Education), Northeast Forestry University, 26 Hexing Road, Harbin 150040, China

² College of Furnishing and Industrial Design, Nanjing Forestry University, Nanjing 210037, China

input. However, characterizing the pore structure of wood can be very difficult because of the wide pore size range and complex pore system.

Currently, the state-of-the-art characterization techniques to analyze porous structures typically include scanning electron microscopy (SEM), X-ray computer tomography (XCT), gas adsorption methods (GAMs) and mercury injection porosimetry (MIP) (Guo et al. 2020; Rajagopal et al. 2019; He et al. 2017, 2020; Li et al. 2017a; Yin et al. 2015; Zauer et al. 2014; Plötze and Niemz 2011). However, all of the aforementioned techniques have limitations in characterizing the porous structure of wood. For example, SEM is a direct observation method that fails to provide quantitative data in three-dimensions (3D). XCT is an expensive technique that typically struggles to recognize pore diameters < 50 nm. The information derived from GAMs is typically related to nanopores only, and hence, provides only a narrow range of information. Finally, the measurement accuracy of traditional MIP is influenced by the hypothesis concerning connecting cylinders.

Compared with other methods, despite the shortcomings, MIP functions on a simple principle with a rapid detection speed across a wide aperture size range. Hence, MIP has been widely applied to the characterization of porous structures of numerous porous materials including wood and rock (Plötze and Niemz 2011; Zauer et al. 2014; Li et al. 2017b; Kong et al. 2019). However, the aforementioned studies of the porous structures typically focused on the porosity or pore size distribution extracted from MIP data. However, there are other important parameters, i.e., threshold pressure and the pore-to-throat ratio, which are beneficial to further elucidate the porous structure. For example, the threshold pressure is the point on the capillary pressure curve at which mercury first intrudes into the pores of the sample, denoting the largest accessible pore size that mercury can ingress into (Nabawy et al. 2009). Even though numerous research efforts have been devoted to elucidating structural information of porous materials by MIP, reports on the use of MIP data to elucidate the porous structure of wood are relatively scarce.

The microporous structures of wood are demonstrated to exhibit a complex nature with a wide range of pore sizes. Additionally, the complex nature of the porous structures gives rise to challenges when modeling using traditional Euclidean geometry. Fractal theory, which was introduced by Mandelbrot (1984), has now become a powerful tool to characterize porous structures. According to the theory of fractal geometry, the fractal dimension of a surface varies between 2.0 and 3.0. If the fractal dimension value is close to three, the porous structures are indicated to be highly complex. The majority of research in this area employs the box-counting method to calculate the fractal dimensions via SEM imaging (Li et al. 2013, 2016). However, fully interpreting the complex structural information is not possible from the fractal dimensions calculated from the maximum and minimum aperture sizes. Numerous reports calculate the fractal dimensions via MIP data, which demonstrate a linear relationship between pressure and saturation (Kong et al. 2019). The fractal dimension can be directly calculated from the slope of this cross-plot. This method of calculating the fractal dimension is widely applied in numerous fields. However, to the best of the authors' knowledge, this is the first report detailing the porous structures of wood by a combination of MIP data and fractal theory.

Hence, the purpose of the study herein is to: (1) take MIP measurements on wood samples and to analyze the MIP data in detail, (2) determine the fractal characteristics of the porous structures derived from the MIP measurements, (3) establish a fractal-structural parameter relationship. The strategy adopted herein can elucidate and quantify the porous structure and also provide the structural parameters needed for future numerical modeling of the macroscopic physical properties.

Materials and methods

Materials

Four tree species (larch, poplar, white birch and oak) from the Greater Khingan area in the Heilongjiang Province of China, were investigated in this study. Although the purpose of this study is to undertake a comprehensive analysis of the porous structures of the woods via MIP, the differences among the different species will be discussed in a follow-up study. The different species are numbered as: larch (sample 1), poplar (sample 2), white birch (sample 3) and oak (sample 4). The porosity of the tree samples ranges from ~40 to 70%. Specimens (about $3 \times 3 \times 3$ mm) were first vacuum dried at 70 °C in an oven for > 10 h and thereafter, sealed inside a desiccator at room temperature until ready for the MIP test. To ensure the reliability of data, each test, for each species, was performed in duplicate.

Methods

MIP test

MIP was performed using an AutoPore IV 9500 instrument (Micromeritics Instrument Corporation, USA) to obtain the textural properties of the wood, including pore volume, porosity and aperture size distribution. First, the oven-dry specimen was placed inside a chamber and isolated. Thereafter, measurements were started by increasing the pressure from 0.1 psia to 60,000 psia (413.68 MPa) on a sample immersed in the non-wetting mercury. The equilibrium time for each pressure increment was set at 10 s. The rate of pressure increase was automatically adjusted using an advanced procedure with lower rates at lower pressure levels and during measured intrusion processes. With increasing pressure, mercury intrudes progressively from big voids to small voids. The timescale of each scan is ~30 min. After the scan, the pore volume can be derived from the quantity of intruded mercury. The pore size distribution can be determined according to the Washburn equation, which gives a relationship between pressure and pore size (Washburn 1921):

$$r = -\frac{2\gamma \cdot \cos \theta}{p} \quad (1)$$

where r is pore radius, p is pressure, $\gamma = 0.48$ N/m and is the surface tension of mercury, $\theta = 140^\circ$ and is the wetting angle of mercury.

The calculation formulas of the other parameters, i.e., porosity φ , aperture size distribution $D(r)$, threshold pressure p_t and pore-to-throat ratio R are given as below:

$$\varphi = \frac{V_T}{V_s} \quad (2)$$

$$D(r) = \frac{p \, dV}{r \, dp} \quad (3)$$

$$R = \frac{D_I}{D_E} \quad (4)$$

where V_T is the total amount of mercury, V_s is the total sample volume, and D_I and D_E are the modal throat and pore sizes, respectively. The threshold pressure p_t is recorded by the device automatically.

The detailed calculation procedure can be observed in the Quantachrome Instrument (2009) operation manual.

Morphology observations using SEM

To observe the pore morphology of the wood cross sections, specimens were cut into samples having dimensions of approximately 5×5 mm, with the sample surfaces smoothly cut. Thereafter, the samples were coated with gold ions using an ion sputtering apparatus and observed by SEM at an acceleration voltage of 20 kV and $400 \times$ magnification (FEI Quanta 200, The Netherlands).

Fractal dimensions

The number of pores (radius $> r$) can be expressed by the following formula on the basis of the fractal principle (Mandelbrot 1984):

$$N(> r) = \int_r^{r_{\max}} P(r) dr = ar^{-D} \quad (5)$$

where r_{\max} is the maximum pore radius, $P(r)$ is the distribution density function of the pore radius, a is a proportionality constant, and D is the fractal dimension.

If the pores are assumed as collections of capillary tubes with radius r , and the radius is equal to the length of the tube l , then the pore volume can be calculated as:

$$V = N\pi r^3 = a\pi r^{3-D} \quad (6)$$

Then,

$$\frac{dV}{dr} = a(3 - D)\pi r^{2-D} \quad (7)$$

Therefore, the total pore volume of the wood with pore sizes $< r$ will be:

$$V(< r) = \int_{r_{\min}}^r a(3-D)\pi r^{2-D} dr = a\pi(r^{3-D} - r_{\min}^{3-D}) \quad (8)$$

In this regard, the total pore volume can be expressed as:

$$V = \int_{r_{\min}}^{r_{\max}} a(3-D)\pi r^{2-D} dr = a\pi(r_{\max}^{3-D} - r_{\min}^{3-D}) \quad (9)$$

Therefore,

$$1 - S_g = \frac{V(< r)}{V} = \frac{r^{3-D} - r_{\min}^{3-D}}{r_{\max}^{3-D} - r_{\min}^{3-D}} \quad (10)$$

where S_g is the mercury saturation, and if $r_{\min} \ll r$, the following equation can be obtained as:

$$1 - S_g = \frac{r^{3-D}}{r_{\max}^{3-D}} \quad (11)$$

The capillary pressure is known to be inversely proportional to the radius of the pores based on the modified Young–Laplace equation. As P decreases, r increases to a maximum value; therefore, the equation can be described as:

$$1 - S_g = \frac{P^{3-D}}{P_{\min}^{3-D}} \quad (12)$$

By taking the logarithm of both sides of the above equation, the following relationship is established:

$$\log(1 - S_g) = (3 - D) \log P - (3 - D) \log P_{\min} \quad (13)$$

Hence, a linear relationship between $\log(1 - S_g)$ and $\log P$ is created and the fractal dimension can be directly calculated from the slope of this cross-plot.

Results and discussion

MIP analysis

The mercury intrusion curves of the four tree samples are shown in Fig. 1, which include the cumulative intrusion and extrusion curves. To further demonstrate the differences in mercury intrusion, the incremental mercury intrusion curves as a function of pressure are also given.

As the intrusion pressure increases, the mercury is first forced into the larger pores at lower pressures, followed by ingress into the smaller pores at higher pressures. The related cumulative mercury intrusion uptake increases, and the magnitude of the uptake is structure dependent.

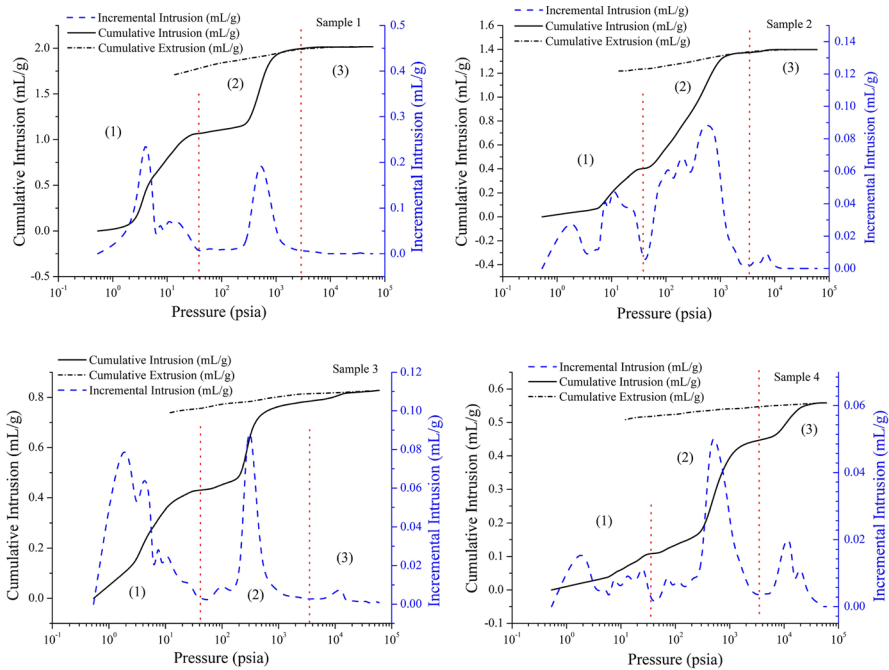


Fig. 1 Mercury intrusion curves as a function of pressure of the wood samples. Larch (sample 1), poplar (sample 2), white birch (sample 3) and oak (sample 4)

For sample 1, when the intrusion pressure reaches a threshold pressure of 3.02 psia, that is the point on the capillary pressure curve where mercury first intrudes into the pores of the sample. As the pressure increases, mercury uptake increases rapidly because of the presence of macropores. When the intrusion pressure reaches 29.96 psia, the increase in mercury uptake tends to plateau suggesting that the ingress of mercury is now transitioning from the macropores to the mesopores. After the breakthrough pressure related to the mesopore size distribution, mercury uptake rapidly increases. At these pressures, mercury flows mainly within mesoscopic pores. Finally, as the pressure is further increased to, and beyond, 1497.10 psia, mercury begins to enter the smaller micropores. However, the pores are extremely difficult to penetrate, and hence, the mercury uptake plateaus again until the pores are filled entirely. As a result of the differences in the structures of the different samples, the mercury uptake curves appear differently (Fig. 1).

From the SEM observations of the four samples (Fig. 2), the mercury injection data correlate to the structural information observed in the micrographs. For example, the pore arrangement and pore size distribution of sample 1 exhibit a higher degree of uniformity than the other samples. Correspondingly, the change of cumulative intrusion and the incremental mercury intrusion curves appear less complicated when compared with the other samples. Subsequent analysis—the threshold pressures and the mercury withdrawal efficiencies—can be used to support the aforementioned phenomenon.

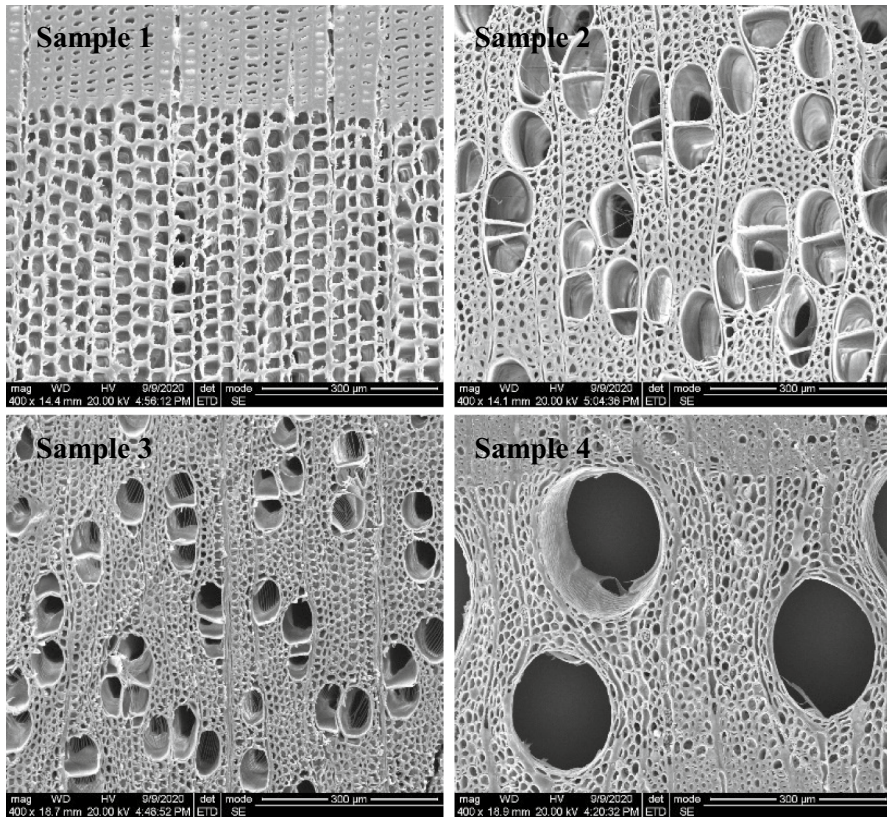


Fig. 2 Scanning electron microscopy images of the four samples

Theoretically, the threshold pressure or breakthrough pressure is the point on the capillary pressure curve where mercury first intrudes into the pores of the sample and is a preliminary indication of the aperture size. Typically, the lower the threshold pressure, the easier for mercury to enter the pores. From Table 1, a low threshold pressure of 3.02 psia corresponds to a higher uptake of mercury per unit mass (2.02 mL/g), which indicates higher levels of porosity (73.18%).

Recently, the threshold pressure was further described by Hu et al. (2017) and extended to explain a connected pore network. Namely, each change in threshold pressure is an indicator of mercury entering a different aperture size. The threshold pressure can be obtained from the inflection point derived from the plot of incremental mercury intrusion versus intrusion pressure on a logarithmic scale. In Fig. 1, incremental mercury intrusion illustrates that each sample has several inflection points, demonstrating that different porous networks exist in the samples. Typically, the higher the number of inflection points, the higher the degree of complexity of the porous structure. The number of threshold pressures of the four samples is 5, 8, 7 and 10, respectively.

Table 1 Pore structure parameters from mercury intrusion data

Sample	Relative pore volume/%			P_t /psia	V_T /mL/g	r_{av} /μm	ϕ /%	R_{av}
	Macropore	Mesopore	Micropore					
	350 μm	5 μm	60 nm					
	I	I	I					
	5 μm	60 nm	2 nm					
1	52.51	44.76	2.73	3.02	2.02	60.4	73.18	160.02
2	28.63	69.14	2.23	6.95	1.40	182.6	64.75	175.27
3	48.59	37.52	13.89	7.01	0.83	218.8	54.54	180.82
4	19.62	58.93	21.45	7.46	0.56	241.8	44.26	211.43

P_t threshold pressure, V_T total amount of mercury, r_{av} average aperture, ϕ porosity, R_{av} average pore-to-throat ratio

For the extrusion curves, the cumulative intrusion value of all the samples decreases as a function of decreased extrusion pressure. Hysteresis is observed between the intrusion and the extrusion curves for all samples. If all pores are ideally uniform and cylindrical in shape and the contact angles of the intrusion and extrusion processes are known, then the hysteresis phenomenon should not be expected since the intrusion and extrusion processes are controlled by the same mechanism and exactly known parameters (Webb 2001). However, as mercury egresses from the porous system, new mercury interfaces are created, and therefore, additional energy is required to remove the mercury out of the pores. During the intrusion process, a pore is filled with mercury not only as a result of the pore size being equal to, or larger than, the corresponding pressure, but also because of a continuous path that mercury needs to follow to arrive at that specific pore. The large internal pores, which are surrounded by smaller pores, can only be filled when the pressure is sufficient to facilitate a pathway for the mercury to arrive at the pore and for the pore in question to be filled completely. During the extrusion process, the reverse phenomenon occurs. The filled pores within the internal structure or isolated pores, will remain filled with any trapped mercury if there is no continuous path toward the sample surface to allow for egress of mercury from the pores (Giesche 2006). Principally, the mercury intrusion and extrusion processes in and out of the pores are controlled by the pore radii and pore connectivity. A larger hysteresis between the mercury intrusion and extrusion processes indicates a higher degree of complexity. The mercury withdrawal efficiency (the ratio of mercury extrusion and intrusion) of the four samples is 16.9%, 12.9%, 10.9% and 9.1%, respectively.

The pore-to-throat ratio is another important parameter for evaluating pore structures (Hemes et al. 2015). In the pore network model (PNM), the large pores/cavities are often modeled as spheres, and the long narrow channels connecting the spheres are considered to be cylinders. PNM approximates the complex porous structure of the wood into pores and connecting channels (throats) of different sizes. The way that pores and throats are connected defines the “topology” of the network. The pore-to-throat ratio can be used to characterize the relationship between the pore and

throat radii, which indicates the degree of ease for mercury intrusion from one state to the next.

Figure 3 shows the pore-to-throat ratio curves of the four tree samples. The pore-to-throat ratios for all samples decrease as a function of increased pressure. However, different amplitudes of variation are observed, which is exactly expected because of the disappearance of large aperture sizes with increased pressure. A closer look at Fig. 3 shows that the pore-to-throat ratio is not extended across the entire pore aperture size range. The endpoint is ~ 10 psia. This phenomenon is related to its definition ($R = \frac{D_I}{D_E}$). Based on the PNM theory and the mercury injection model, the mercury uptake curve mainly depicts information pertaining to the pore aperture; however, the mercury ejection curve principally provides information on the throat radius. The pore-to-throat ratio curves follow both the mercury intrusion and extrusion curves. Because the extrusion curve is not extended across the entire pore size range, the occurrence of the pore-to-throat ratio corresponds to the mercury ejection curve. The average pore-to-throat ratio is given in Table 1, which is used to establish a relationship with the fractal dimension.

To obtain the aperture size distribution, differential intrusion $\frac{dV}{dr}$ and log differential intrusion $\frac{dV}{d(\log r)}$ are calculated. As a result of the large aperture size range, approximately from ~ 1 nm to 10^6 nm, the forms of the pore size distribution expressions are different. Hence, the different forms of expressions ($\frac{dV}{dr}$ and $\frac{dV}{d(\log r)}$) should be used to eliminate the effect of magnitude, which is a common data processing means in MIP. Figure 4 shows pore size distributions of the four tree samples. For the differential intrusion curves, the distributions with apertures $< 10^3$ nm are shown. Except for sample 3, the other samples exhibit bimodal distributions. For the log differential intrusion curves, the distributions with aperture sizes $> 10^3$ nm are shown. The distributions of all samples are approximately bimodal. Hence, from the

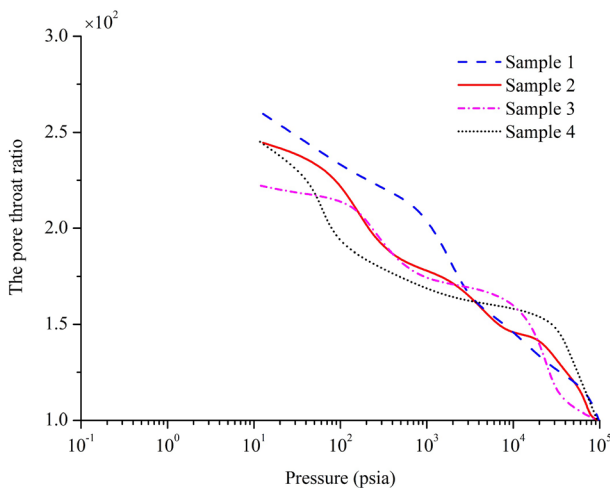


Fig. 3 Pore-to-throat ratio curves of the wood samples

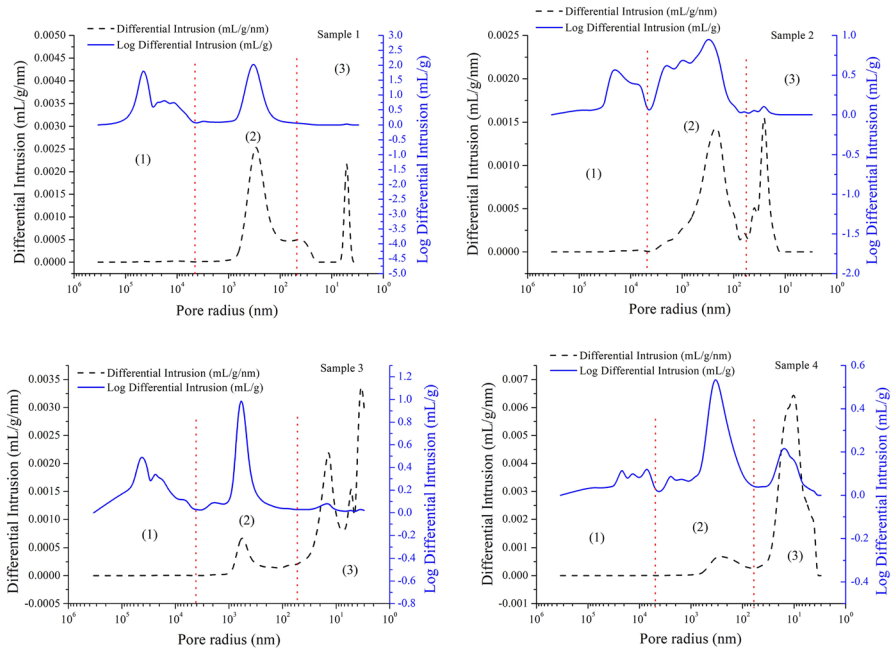


Fig. 4 Pore size distributions of the wood samples

differential intrusion and log differential intrusion curves, three pore size groupings are clearly distinguished: macropores (radius 350–5 μm), mesopores (5 μm –60 nm), and micropores (60–2 nm). The relative pore volumes and other parameters are presented in Table 1. From the relative pore volumes, there are different proportions among the macropores, mesopores and micropores. Accordingly, each pore size classification contributes differently to the macro properties (Wang et al. 2018). Hence, structural information at each pore size classification should be represented separately, i.e., calculation of the fractal dimension that will be discussed in fractal analysis section.

Fractal analysis

To present the fractal characteristics of the porous structures in the samples based on the mercury injection analysis, the cross-plot of $\log(1 - S_g) - \log(P_c)$ for all samples was constructed. Figure 5 shows the fractal dimension for each corresponding aperture range intervals of the four samples. The data demonstrate a good fit with a high correlation coefficient that indicates that the porous structures exhibit fractal behavior. The curves from all the four samples can be divided into three segments, as shown by the different color representations in Fig. 5, the smallest absolute value for the slope represents the macropores, while the largest absolute value of the slope can denote the micropores. The remaining segment, which has the absolute value in between the macropores and micropores, relates to the mesopores. The fractal

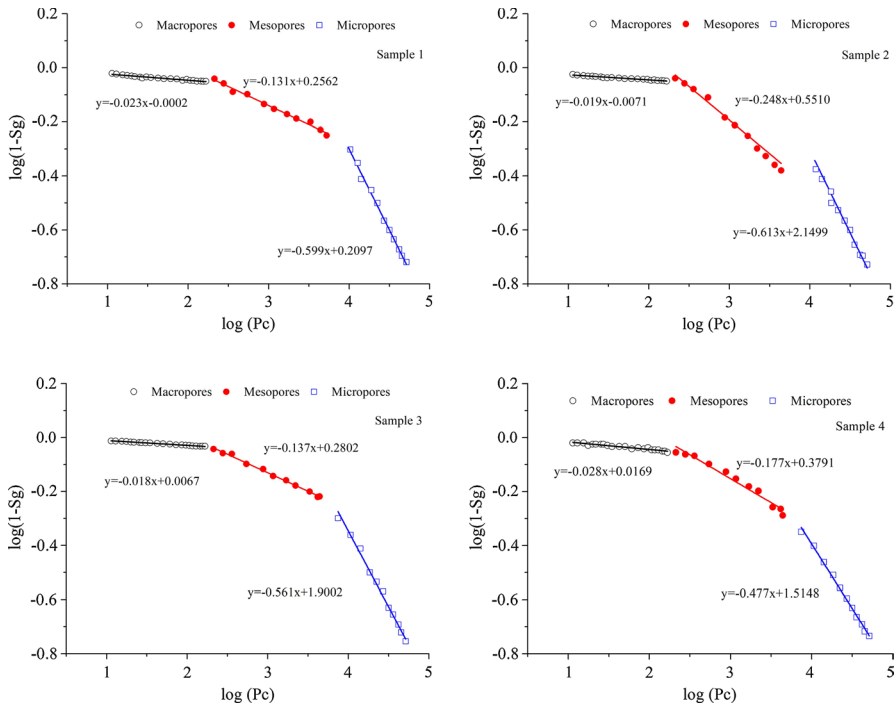


Fig. 5 Fractal dimension of the four tree samples

analysis results of all samples are presented in Table 2. The fractal dimension D_{macr} varies between 2.972 and 2.982 with an average value of 2.978. D_{meso} varies between 2.752 and 2.869 with an average value of 2.827. D_{micr} varies between 2.387 and 2.523 with an average value of 2.438. As observed, D_{macr} , which reflects the larger pores in each of the four samples exhibits a fractal dimension value closer to 3.0, while D_{micr} , which represents the smaller pores has a fractal dimension value closer to 2.3. The fractal dimension values follow: $D_{\text{macr}} > D_{\text{meso}} > D_{\text{micr}}$, indicating that the complexity of the micropores in these samples is overall less than the complexity for both the mesopores and macropores. These results are consistent with the mercury injection data and SEM observations. From Fig. 2, the macropore distribution

Table 2 Fractal analysis of the four tree samples

Wood sample	Macropore		Mesopore		Micropore		All D
	D_{macr}	R^2	D_{meso}	R^2	D_{micr}	R^2	
1	2.977	0.954	2.869	0.974	2.401	0.979	2.790
2	2.981	0.973	2.752	0.992	2.387	0.982	2.813
3	2.982	0.990	2.863	0.989	2.439	0.991	2.888
4	2.972	0.931	2.823	0.969	2.523	0.996	2.893
Average	2.978	0.962	2.827	0.981	2.438	0.987	2.846

appears highly random. The incremental mercury intrusion curves within the macropore region fluctuate significantly (Fig. 1). This phenomenon is also observed in other porous materials, where multifractal characteristics of the pores/throats in Bakken Shale show that the complexity of the macropores is obviously higher than the complexity of the micropores (Liu et al. 2019). At the same time, Zheng et al. (2018) reported that the complexity of the macropores significantly influences the permeability of coals by nuclear magnetic resonance studies and fractal analysis theory.

Based on the weighted average of the porosity from the macropores, mesopores and micropores, the weighted fractal dimension D_w across the entire pore range was calculated by (Li et al. 2017b):

$$D_w = \varphi_{\text{macr}} D_{\text{macr}} + \varphi_{\text{meso}} D_{\text{meso}} + \varphi_{\text{micr}} D_{\text{micr}} \quad (14)$$

where D_{macr} , D_{meso} , D_{micr} are fractal dimensions, which can be observed in Table 2. φ_{macr} , φ_{meso} , φ_{micr} are the relative proportions of macropores, mesopores and micropores, respectively, which can be observed in Table 1. The weighted fractal dimension will be used to establish the relationship with the porous structural parameters, which is discussed in fractal dimension-structural parameter relationship analysis section.

Fractal dimension-structural parameter relationship analysis

Prior to analyzing the fractal dimension-structural parameter relationship, the relationship between the pore structure parameters should first be discussed. Figure 6 shows the relationship between porosity and the average aperture size and average pore-to-throat ratio. As observed from the above data, porosity exhibits a strong

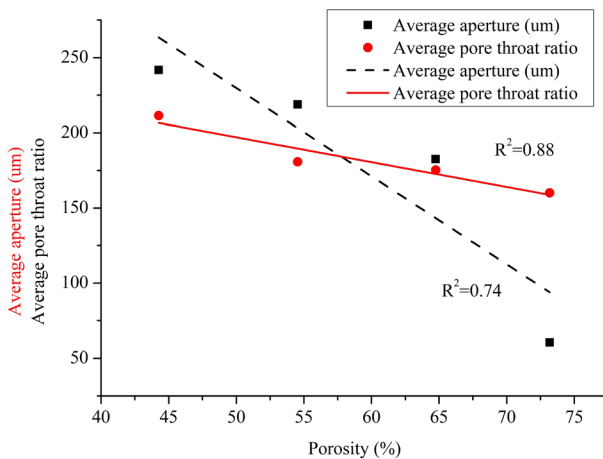


Fig. 6 Relationships between porosity and the average aperture size and pore-to-throat ratio

negative correlation with an average aperture size and average pore-to-throat ratio having corresponding R^2 values of 0.74 and 0.88, respectively.

This phenomenon is consistent with expectations. Typically, the pore size increases, to a certain degree, as a function of porosity. However, herein, although the porosity of sample 1 is highest (Table 1), the pore size distribution is narrow (Fig. 2). Accordingly, the average aperture size is relatively small. However, for the other samples, because of the presence of catheters, the average aperture size is increased. Nevertheless, as a result of having smaller proportions (Table 1), the contribution to the overall porosity is low. Hence, porosity shows a negative correlation with average aperture size.

The average pore-to-throat ratio is observed to be principally influenced by pore size. According to the wood anatomy, the difference of micropore size, especially for nanopores, among the different tree species, is relatively small (Liu and Zhao 2006). According to the definition of the pore-to-throat ratio (R), the modal throat size (small pores) is approximately constant, and accordingly, R is determined by the modal pore size (large pores). Hence, the increase in the average aperture size leads to an increase in the average pore-to-throat ratio (Fig. 7).

The relationships between the structure parameters (porosity, average aperture size and pore-to-throat ratio) and fractal dimension are established in Fig. 8.

Statistically speaking (Cohen 2013), when the correlation coefficient is < 0.4 there is no correlation in theory. The correlation is considered to be weak when the correlation coefficient is between 0.4 and 0.8. For a correlation coefficient > 0.8 , a significant correlation is observed. Fortunately, all correlation coefficient values observed herein are > 0.4 , as shown in Fig. 8, indicating a correlation between the structural parameters and the fractal dimension. The negative correlations between the fractal dimension and porosity exhibit R^2 values of 0.85. Furthermore, the positive correlations observed between the fractal dimension and the average pore radius and pore-to-throat ratio have R^2 values of 0.66 and 0.52, respectively.

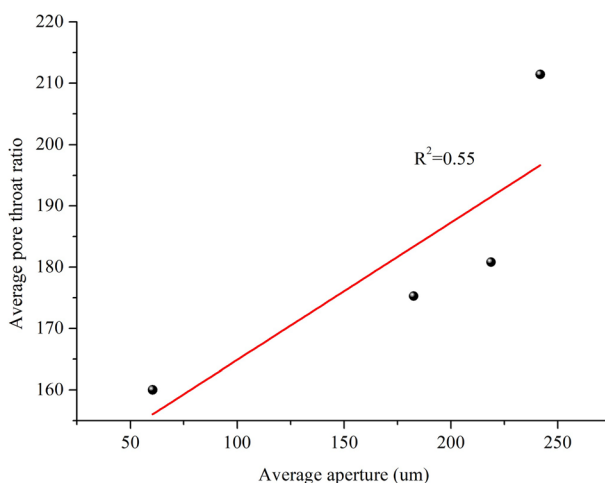


Fig. 7 Relationship between the average aperture size and the pore-to-throat ratio

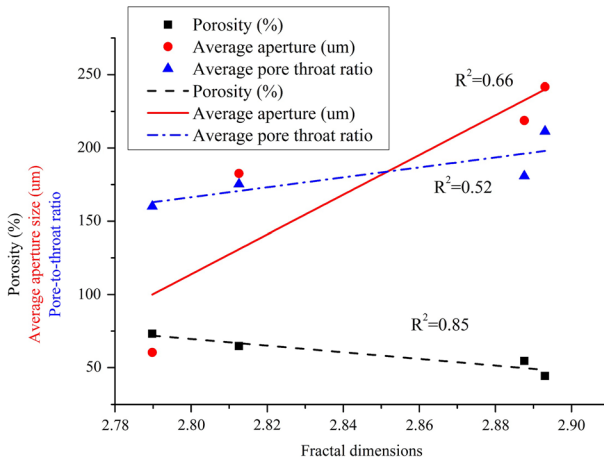


Fig. 8 Relationships between fractal dimension and porosity, average aperture size and pore-to-throat ratio

As observed from the above data, porosity shows a strong negative correlation with fractal dimension, which suggests the complexity of the porous structure is largely affected by the porosity. Typically, in the field of porous materials, increased porosity may increase the probability of porosity arrangement complexity. However, herein, although the porosity of sample 1 is highest (Table 1), the pore size distribution is narrow (Fig. 2). Hence, sample 1 exhibits a low complexity and small fractal dimension (Table 2). Similar results have been reported in other studies, i.e., wood-strand composites (Li et al. 2016).

For the relationships between fractal dimension and the average pore radius and pore-to-throat ratio, the correlation is suggested to be related to the size and arrangement of the pores (Fig. 2). Conversely, larger pore size differences and unordered arrangements promote a more complex wood structure. As observed from the above analysis, although porosity and fractal dimension have a significant correlation, the nature of the complexity that determines the wood structure is related to the size and arrangement of the pores.

Discussions

Herein, the MIP data were analyzed from different perspectives. The fractal characteristics of the porous structures were derived from the MIP data. The relationship between the pore structure parameters and the fractal-structural parameter was analyzed. However, further research and discussions will be presented in a follow-up study to provide further elucidation. For example: (1) herein, the MIP data proposed by Quantachrome were directly used to analyze the pore structure characteristics. The MIP model is assumed based on cylindrical and connected pores. Hence, there is a need to clarify the suitability of the model to obtain the correct data with respect to the wood structure. (2) The 3D fractal calculation method used herein is based

on MIP data. However, using 2D SEM data to validate 3D fractal data may be inadequate. Hence, the choice of the 3D pore structure characterization method, that is, XCT in situ loading techniques, is recommended to detail the specific position at which mercury actually enters the wood as a function of pressure. (3) There are numerous ways to calculate fractal dimension, hitherto, based on different models (Wang et al. 2019; Sun et al. 2019). However, further discussions are required to elucidate which model is more suited to characterize the complexity of the wood pore structure. Unfortunately, there are few reports detailing the above in the wood field. Hence, further research in this area is required.

Conclusion

MIP, as a widely used technique to study porous structures, was applied in this study to analyze four tree samples from larch, poplar, white birch and oak. Numerous structural and textural properties such as porosity, aperture size distribution, threshold pressure, pore-to-throat ratio and fractal dimension were analyzed. Based on this study, a few conclusions can be made: (1) detection aperture ranged from about 2.0 nm to 350 μm . Porosity ranges from 44.26 to 73.18%. According to the mercury intrusion curves and distributions of pore aperture, three pore size classes could be distinguished: macropores (radius 350–5 μm), mesopores (5 μm –60 nm) and micropores (60–2.0 nm). (2) The threshold pressure, average pore radius and pore-to-throat ratio extracted from the MIP data can be used as a valid parameter to evaluate the structural characteristics. For example, the obtained values, to a certain degree, can indicate the ease of mercury intrusion, which indirectly reflects the structural complexity. (3) The fractal dimension values in the corresponding macropore, mesopore and micropore aperture range intervals are 2.978, 2.827 and 2.438, respectively, which indicate a higher degree of pore complexity for larger pores. (4) Negative correlations are observed between the fractal dimension and porosity with R^2 values of 0.85, and in addition, positive correlations are observed between the fractal dimension and the average pore radius and pore-to-throat ratio with corresponding R^2 values of 0.66 and 0.52, respectively.

Acknowledgements The project was supported by the “National Natural Science Foundation of China”, Grant Nos.: 31901242 and 31870545. We thank Liwen Bianji, Edanz Editing China (www.liwenbianji.cn/ac), for editing the English text of a draft of this manuscript.

Compliance with ethical standards

Conflict of interest On behalf of all authors, the corresponding author states that there is no conflict of interest.

References

- Cohen J (2013) Statistical power analysis for the behavioral sciences. Academic press, New York
- Giesche H (2006) Mercury porosimetry: a general (practical) overview. Part Part Syst Char 23:9–19
- Guo L, Cheng H, Chen J, Chen W, Zhao J (2020) Pore structure characterization of oak via X-ray computed tomography. BioResources 15:3053–3063

- He S, Xu J, Wu Z, Bao Y, Yu H, Chen Y (2017) Compare of porous structure of moso bamboo and *Pinus sylvestris* L. lumber. *J Nanjing For Univ Nat Sci Edit* 41:157–162
- He S, Chen Y, Wu Z, Bao Y, Yu H (2020) Research progress on wood/bamboo microscopic fluid transportation. *J For Eng* 5:12–19
- Hemes S, Desbois G, Urai JL, Schröppel B, Schwarz J-O (2015) Multi-scale characterization of porosity in Boom Clay (HADES-level, Mol, Belgium) using a combination of X-ray μ -CT, 2D BIB-SEM and FIB-SEM tomography. *Micropor Mesopor Mat* 208:1–20
- Hu Q, Zhang Y, Meng X, Li Z, Li M (2017) Characterization of micro-nano pore networks in shale oil reservoirs of Paleogene Shahejie Formation in Dongying Sag of Bohai Bay Basin, East China. *Pet Explor Dev* 44:720–730
- Kong L, Ostadhassan M, Liu B, Li C, Liu K (2019) Multifractal characteristics of MIP-based pore size distribution of 3D-printed powder-based rocks: a study of post-processing effect. *Transp Porous Med* 129:599–618
- Li P, Wu Q, Tao Y (2013) Fractal dimension analysis of void size in wood-strand composites based on X-ray computer tomography images. *Holzforschung* 67:177–182
- Li P, Tao Y, Wu Q (2016) A three-dimensional void reconstruction method for analyzing fractal dimensions of void volume in wood-strand composites. *Holzforschung* 70:377–382
- Li L, Wang X, Yan Y, Ping L (2017a) Pore analysis of thermally compressed Scots pine (*Pinus sylvestris* L.) by mercury intrusion porosimetry. *Holzforschung* 72:57–63
- Li P, Zheng M, Bi H, Wu S, Wang X (2017b) Pore throat structure and fractal characteristics of tight oils and stone: a case study in the Ordos Basin, China. *J Pet Sci Eng* 149:665–674
- Liu Y, Zhao G (2006) Wood resources and materials science. China Forestry Press, Beijing
- Liu K, Ostadhassan M, Kong L (2019) Fractal and multifractal characteristics of pore throats in the Bakken Shale. *Transp Porous Med* 126:579–598
- Mandelbrot BB (1984) The fractal geometry of nature, vol 173. WH freeman, New York
- Nabawy BS, Géraud Y, Rochette P, Bur N (2009) Pore-throat characterization in highly porous and permeable sandstones. *AAPG Bull* 93:719–739
- Plötze M, Niemz P (2011) Porosity and pore size distribution of different wood types as determined by mercury intrusion porosimetry. *Eur J Wood Prod* 69:649–657
- Quantachrome Instrument (2009) The operation manual of mercury porosimetry analyzer. <https://www.quantachrome.com>
- Rajagopal H, Khairuddin ASM, Mokhtar N, Ahmad A, Yusof R (2019) Application of image quality assessment module to motion-blurred wood images for wood species identification system. *Wood Sci Technol* 53:967–981
- Sun H, Mañín D, Najser J, Neděla V, Navrátilová E (2019) Fractal characteristics of pore structure of compacted bentonite studied by ESEM and MIP methods. *Acta Geotech* 15:1–17
- Wang X, Hou J, Song SH, Wang DM, Gong L, Ma K (2018) Combining pressure-controlled porosimetry and rate-controlled porosimetry to investigate the fractal characteristics of full-range pores in tight oil reservoirs. *J Petrol Sci Eng* 171:353–361
- Wang F, Yang K, You J, Lei X (2019) Analysis of pore size distribution and fractal dimension in tight sandstone with mercury intrusion porosimetry. *Results Phys* 13:102283
- Washburn EW (1921) Note on a method of determining the distribution of pore sizes in a porous material. *P Natl Acad Sci USA* 7:115
- Webb PA (2001) An introduction to the physical characterization of materials by mercury intrusion porosimetry with emphasis on reduction and presentation of experimental data Micromeritics Instrument Corp. Norcross, Georgia
- Yin J, Song K, Lu Y, Zhao G, Yin Y (2015) Comparison of changes in micropores and mesopores in the wood cell walls of sapwood and heartwood. *Wood Sci Technol* 49:987–1001
- Zauer M, Hempel S, Pfriem A, Mechtcherine V, Wagenführ A (2014) Investigations of the pore-size distribution of wood in the dry and wet state by means of mercury intrusion porosimetry. *Wood Sci Technol* 48:1229–1240
- Zheng S, Yao Y, Liu D, Cai Y, Liu Y (2018) Characterizations of full-scale pore size distribution, porosity and permeability of coals: a novel methodology by nuclear magnetic resonance and fractal analysis theory. *Int J Coal Geol* 196:148–215